SCIENCE INSTRUMENTATION CENTRE

(Research Article published using instruments in SIC)

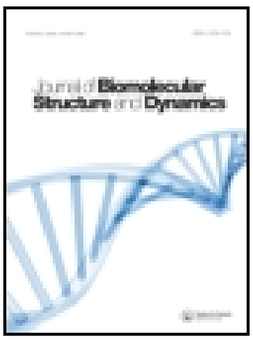

Taylor & Francis
Taylor & Francis Group

Journal of Biomolecular Structure and Dynamics

ISSN: 0739-1102 (Print) 1538-0254 (Online) Journal homepage: https://www.tandfonline.com/loi/tbsd20

In silico and *in vitro studies* of transition metal complexes derived from curcumin –isoniazid Schiff base

Porkodi Jeyaraman, Arunadevi Alagarraj & Raman Natarajan

To cite this article: Porkodi Jeyaraman, Arunadevi Alagarraj & Raman Natarajan (2019): *In silico* and *in vitro studies* of transition metal complexes derived from curcumin –isoniazid Schiff base, Journal of Biomolecular Structure and Dynamics, DOI: 10.1080/07391102.2019.1581090

To link to this article: https://doi.org/10.1080/07391102.2019.1581090

Accepted author version posted online: 15 Feb 2019.

In silico and *in vitro studies* of transition metal complexes derived from curcumin – isoniazid Schiff base

Jeyaraman Porkodi, Alagarraj Arunadevi and Natarajan Raman *

Research Department of Chemistry, VHNSN College, Virudhunagar-626 001, India

**E-mail: ramchem1964@gmail.com; Tel.: +091-092451-65958; Fax: +091-4562-281338*

Abstract

A series of transition metal complexes have been synthesized from biologically active curcumin and isoniazid Schiff base. They are characterized by various spectral techniques like UV-Vis, FT-IR, NMR, EPR and Mass spectroscopy. Moreover, elemental analysis, magnetic susceptibility, and molar conductivity measurements are also carried out. All these data evident that the metal complexes acquire square planar except zinc(II) which adopts a tetrahedral geometry and they are non- electrolytic in nature. Groove mode of binding between the CT DNA and metal complexes is confirmed by electronic absorption titration, viscosity and cyclic voltammetry studies. In addition to that, all the metal complexes are able to cleave pUC 19 DNA. Optimised geometry and ground state electronic structure calculations of all the synthesized compounds are established out by DFT using B3LYP method which theoretically reveals that copper(II) complex explores higher stability and higher biological accessibility. This is experimentally corroborated by antimicrobial studies. *In silico* ADME studies reveal on the biological potential of all synthesized complexes and also biological activity of the ligand is predicted by PASS online biological activity prediction software. Molecular docking studies are also carried out to confirm the groove mode of binding and receptor-complex interactions.

Keywords: Isoniazid; Groove binding; DFT calculation; *In silico* ADME, Molecular docking; Antimicrobial.

1 Introduction

Molecules which are deployed from the biological active ingredients not only enhance their activity but also reduce their adverse effects. Innovation of peculiar and potential analogues from these ingredients plays a vital role in recent medicinal research fields. Among them, Curcumin, a diferuloylmethane yellow pigment extracted from turmeric (*Curcuma longa* L) (Heger *et al.,* 2014) exhibits potential against various dreadful diseases such as cancer, antitumoral, antimicrobial (Niu *et al.,* 2018), anti-inflammatory, antioxidant (Chanphai *et al.,* 2018*)* , antihepatotoxic, antihyperlipidemic, antiviral, and anti-Alzheimer′s diseases (Awasthi *et al* ., 2018). It is also associated with nontoxicity upto high dosages (Cheng *et al.,* 2001; Goel *et al.,* 2008).

Hydrazones are a class of organic compounds with C=N-NH moiety, which is formed by the action of one hydrazine or hydrazide with a ketone or aldehyde. Isoniazid is one of an effective hydrazide, adopted for the treatment of tuberculosis. But it affords some blackballed side effects (Xu *et al* ., 2014). It has been found that, these hydrazones of isoniazid are less toxic with preserving activity which is due to the inactivation of the NH_2 group (Gonzalez-Baro *et al.,* 2012; Ferraresi-Curotto *et al*., 2015). In co-ordination chemistry, they have acquired special deliberation as polydentate ligands (Gonzalez-Baro *et al*., 2017; Maurya *et al*., 2006) and their metal complexes displayed antimicrobial, antituberculosis, antitumoral and antimycobacterial activities (Krishnamoorthy *et al*., 2011; Ferreira *et al* ., 2010; Maccar *et al* ., 2004).

DNA (Deoxyribo Nucleic Acid) disentangle efficiency of the metal complexes has been extensively studied to identify their potential as anticancer drugs (Abdel-Rahman *et al.,* 2010; Shahabadi *et al.,* 2010; Xiong & Ji, 1999; Sigman, 1993; Heinrich *et al.,* 2018). Their interactions with DNA also render a pathway for the development of new antimicrobial and anti-inflammatory agents. Both the metal complexes of curcumin and hydrazones have strong affinity to interact with DNA (Athappan *et al.,* 2005; Fekri *et al.,* 2018). DFT calculation using Gaussian 09W software aids to study the electronic properties and theoretically predicts the biological accessibility of the compounds (Pramanik *et al.,* 2014). *In silico* drug designing abets a way to predict simultaneously more than one thousand biological and toxicological activities by using the structural formulae of the organic compounds (Khan *et al* ., 2017 ; Varadharajan *et al* ., 2018 and Jaykant *et al* ., 2018).

By observance of these particulars in mind, this research work deals with the synthesis of transition metal complexes from novel hydrazones derived from curcumin and isoniazid. They are characterized by elemental analysis, magnetic susceptibility, molar conductivity measurements, UV- Vis, FT-IR, NMR, EPR and Mass spectroscopy. DNA disentangle studies of the synthesized metal complexes are examined. DFT (Density Functional Theory) calculations of the ligand and metal complexes are carried out in Gaussian 09W software. *In silico* ADME (Absortion, Distribution, Metabolism, Excretion) and biological activity prediction analyses are also described. Based on the results, molecular docking studies are done in HEX8.0 software. All the synthesized compounds are screened for antimicrobial activities.

2 EXPERIMENTAL

All the reagents viz., curcumin, isoniazid and metal chloride salts were purchased from Himedia. DNA was purchased from Bangalore Genei (India). Tris–HCl buffer solution (pH 7.2) was used to study the DNA binding and cleavage studies. pUC 19 DNA was purchased from Bangalore.

The technicalities dealing with the instrumentation and materials adopted in the DNA interaction studies, SWISS ADME, DFT calculation, antimicrobial and molecular docking studies are accustomed in Supplementary file (S1).

2.1 Synthesis of curcumin derived hydrazone (L)

Curcumin derived hydrazone was prepared by refluxing equimolar concentration of curcumin and isoniazid in 30 mL of ethanol for *ca* 4 h. 5 drops of glacial acetic acid was added during the course of the reaction to lower the pH to 5. Then the volume of reaction mixture was reduced and washed with petroleum-ether for 3 times. Finally it was poured into water. The red orange precipitate was obtained. Then, it was recrystallized in hot solution of ethanol and dried in *vacuo*. The scheme for the synthesis of curcumin derived hydrazone is shown in Scheme 1.

Yield: 80%. M.Wt: 487.5; Anal. Cald. for [$C_{27}H_{25}N_3O_6$] (%): C 66.52, H 5.17, N 8.62; Found (%) : C 66.12, H 5.12, N 8.5; FT IR (KBr disc cm^{-1}): 1627 (C=O), 1597 (HC=N), 3420 (intra molecular OH), 1373 (OCH_3), 975 (enolic –C-O-), Aliphatic –C=CH stretch,750, 815 and 850. ^{1}H NMR ($CDCl_3$) (δ): (aromatic H) 7-8.5 (m, 8H), (O-CH_3) 3.92

(s, 6H), (N-H) 2.5 (s, 1H), (enolic OH) 10.88, phenolic – OH (s) : 7.9, phenolic – OH (s) : 9.1, active –CH (s) : 5.95, -C=CH on azomethine side (d,d) : 6.5, 6.8, ^{13}C NMR ($CDCl_3$) (δ): (aromatic C) 120-134.8 (m), (O-CH_3) 54 (s), (C=C) 58 (s), 72 (s) (C-H active) (C-OH) 100.2 (s), (C=N) 163.8 (s), (C=O) 182.3 (s); ESI-MS: 487.1 m/z. UV-Vis in DMSO, nm (transition): 285 (π-π*) and 345 (n-π*).

2.2 Synthesis of metal complexes

About equimolar concentration of curcumin derived hydazone and metal(II) chloride [Cu(II)/Ni(II)/Co(II) / Zn(II)] were refluxed in ethanol with stirring for *ca* 3 h. The resulting solution was cooled. The coloured precipitate obtained was filtered, washed in ethanol and dried. It was recrystallized from hot ethanolic solution. The synthetic detail is shown in Scheme 2.

[CuLCl]: Yield: 75 %; Brown colour; Anal. Calc. for [$CuC_{27}H_{24}ClN_3O_6$] (%): C (60.1), H(4.7), N (4.4) and Cu (6.2); Found (%): C (60.6), H (4.8), N (4.4) and Cu (6.7); FT-IR (KBr) (cm^{-1}): 1575 (-C=N), 1615 (C=O), 518 (M-O), 435 (M-N) and 357 (M-Cl); $\wedge_m$ ($\Omega^{-1}mol^{-1}cm^2$) 18.0; μ_{eff} (BM) 1.82; UV-Vis in DMSO, nm (transition): (d-d). 550

[CoLCl]: Yield: 70%; Dark green colour; Anal.Calc for [$CoC_{27}H_{24}ClN_3O_6$](%): C (60.1), H (4.7), N (4.4) and Co (6.1); Found (%): C (60.9), H (4.8), N (4.4) and Co (6.2); FT-IR (KBr) (cm^{-1}): 1580 (-C=N), 1613 (C=O), 520 (M-O), 430 (M-N) and 360 (M-Cl); $\wedge_m$ ($\Omega^{-1}mol^{-1}cm^2$) 17.0; μ_{eff} (BM) 3.17 ; UV-Vis in DMSO,nm (transition): 520 (d-d).

[NiLCl]: Yield: 66%; Orange colour; Anal.Calc for [Ni $C_{27}H_{24}ClN_3O_6$] (%):C (60.2), H (4.7), N (4.4) and Ni (6.0); Found (%): C (60.9), H (4.8), N (4.4) and Ni (6.2); FT-IR (KBr) (cm^{-1}) 1585 (-C=N), 1620 (C=O), 518 (M-O), 430 (M-N) and 359 (M-Cl); $\wedge_m$ ($\Omega^{-1}mol^{-1}cm^2$) 16.0; μ_{eff} (BM) 0; UV-Vis in DMSO, nm (transition): 540 (d-d).

[ZnLCl]: Yield:65%; Orange red colour; Anal.Calc for [Zn $C_{27}H_{24}ClN_3O_6$] (%): C (60.5), H (4.8), N (4.4) and Zn (6.9); Found (%) : C (60.2), H (4.7), N (4.4) and Zn (6.5); FT-IR (KBr) (cm^{-1}): 1590 (-C=N), 1619 (C=O), 525 (M-O), 438 (M-N) and 352 (M-Cl); ^{1}H NMR (DMSO-d_6) δ : 6.5-7.9 (m,Ar-H), 2.6 (s,-N-H), 3.98 (s, -OCH_3); ^{13}C NMR (DMSO-d_6) δ: 121-135 (Ar-C), 159.5(-CH=N), 179.2(C=O), 10.7 (-C-CH_3); $\wedge_m$ ($\Omega^{-1}mol^{-1}cm^2$) 11.0; μ_{eff} (BM) diamagnetic; UV-Vis in DMSO, nm (transition): 365 (LMCT).

3 Results and discussion

Transition metal complexes of curcumin derived hydrazone are fabricated by using the ligand L and metal chloride (Cu(II), Ni(II),Co(II), Zn(II)) in 1:1 ratio. The ligand L is dissolved in common organic solvents like ethanol, methanol and acetonitrile. All the metal complexes are soluble in hot ethanol, DMSO (Dimethyl sulphoxide) and DMF (Dimethyl formamide) . Both the ligand as well as the metal complexes is stable at room temperature. The geometry and the nature of the metal complexes are predicted by various spectroscopic and analytical techniques. Conductivity measurements studies indicate the non-electrolytic nature of metal complexes. The schematic routes for the synthesis of ligand L and metal complexes [MLCl] are presented in Schemes 1 and 2.

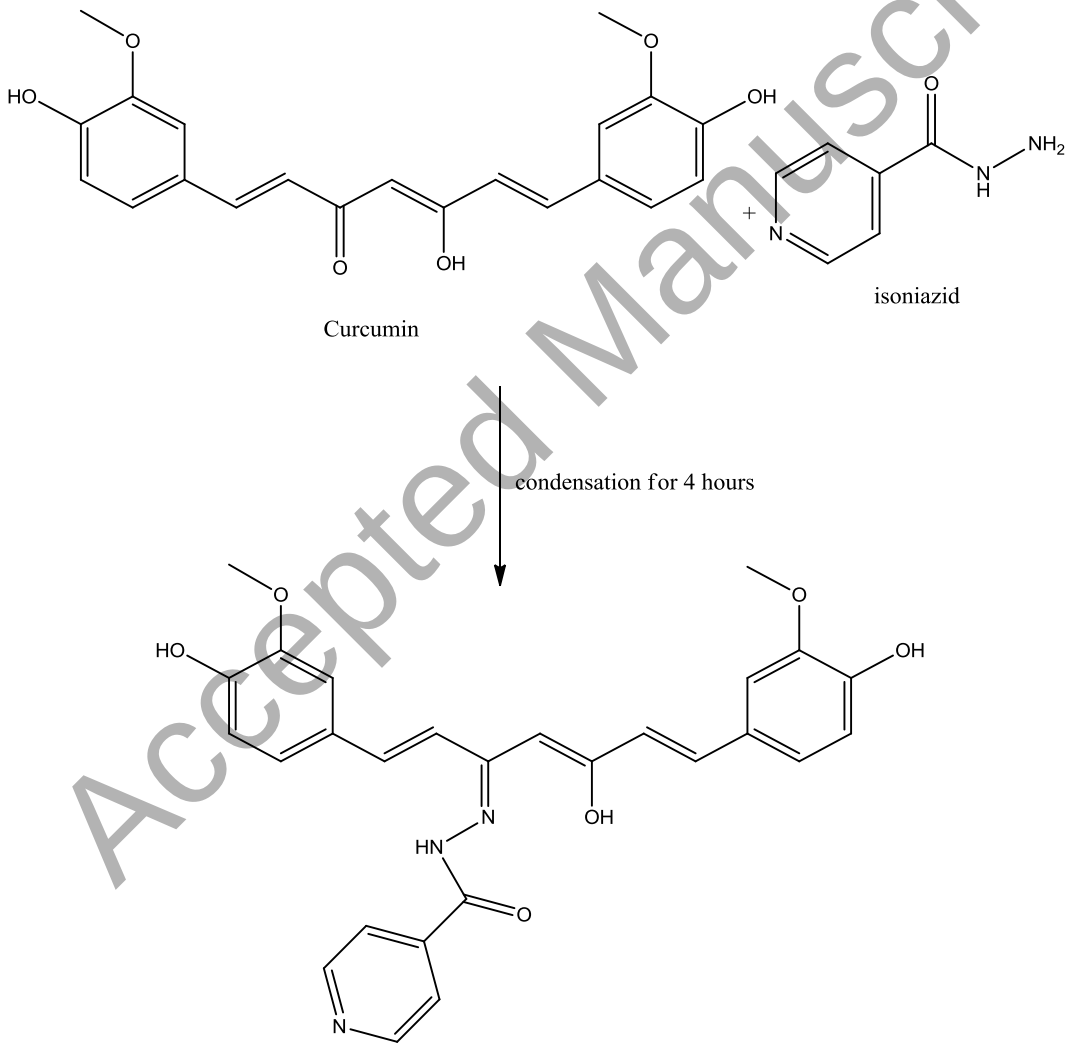

Curcumin derived hydrazone

Scheme 1: Schematic route for the synthesis of curcumin derived hydrazone

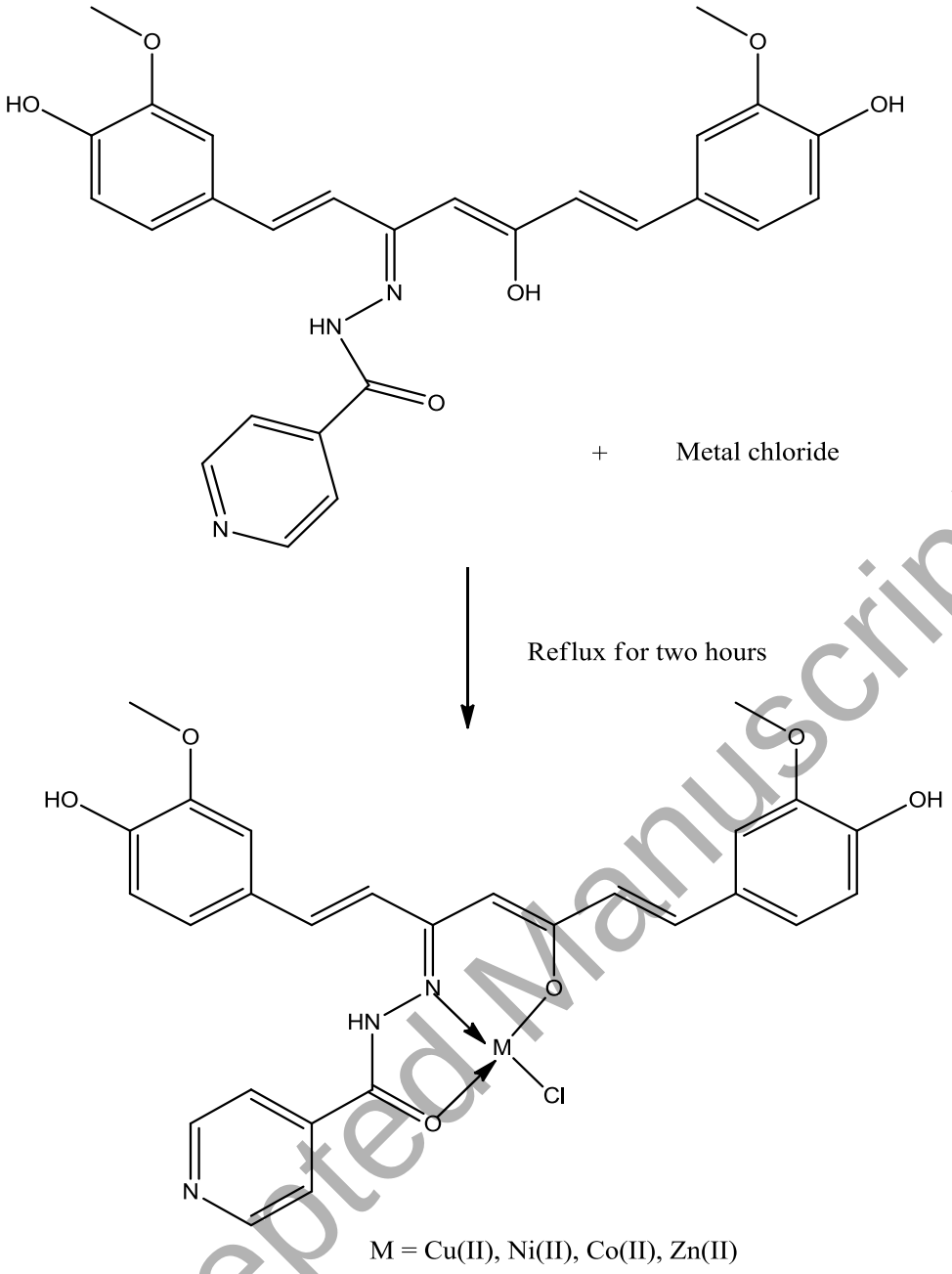

Scheme 2: Schematic route for the synthesis of metal complexes using curcumin derived hydrazone

3.1 Elemental analysis

Both the ligand and metal complexes were subjected to elemental analysis and the results acquired coincide well with the formula of the synthesized metal complexes [MLCl]. Molar conductance was measured for metal complexes in 10^{-3} mol dm^{-3} concentration. The molar conductivity values of the complexes are found to be in the range of 15-18 $\Omega^{-1}cm^2$ mol^{-1}. These lower values reveal the non-electrolytic nature of the metal complexes (Abu-Dief *et al*., 2015; Geary, 1971) and presence of phenolic OH groups in curcumin.

3.2 Electronic spectral and magnetic moment studies

The UV- Vis spectroscopy is used to find out the type of transition and geometry of the metal complexes. The UV – Vis spectra of the ligand and metal complexes are recorded in DMSO solution between 200- 900 nm. In Fig. S1, the ligand L shows two absorption bands, one at 285 nm and another at 345 nm which are due to $\pi \rightarrow \pi^*$ and $n \rightarrow \pi^*$ transitions. These absorption bands indicate that the non – bonding and π electrons are available in ligand L. After complex formation, either of these bands was shifted towards longer wavelength which was due to LCMT (Ligand to metal charge transfer transition). The UV-Vis spectra of copper and cobalt complexes showed d-d transition around 550 nm and 520 nm respectively. These are attributed due to $^2B_{1g} \rightarrow {}^2A_{1g}$ and $^1A_{1g} \rightarrow {}^1B_{1g}$ transitions which are the characteristics bands of square planar geometry (Shebl, 2017; Blasco *et al*., 2010; Nejo *et al*., 2010). The monomeric nature of these complexes was confirmed by their magnetic moment values, 1.82 BM and 3.17 BM. The square planar geometry of nickel complex was also confirmed by its UV-Vis absorption band at 540 nm and zero magnetic moment value (Barbier *et al* ., 1985). Zinc complex does not show d-d transition and because of the d^{10} configurated electronic system. It shows INCT at 365 nm. Its magnetic moment value is also zero because of diamagnetic nature. Due to the lack of d-d transition, Zn(II) complex may adopt tetrahedral geometry instead of square planar geometry. The UV-Vis spectrum of [CoLCl] complex is shown in Fig. S2**.**

3.3 Vibrational spectral analysis

FT IR spectroscopy is a cardinal tool to authenticate the formation of ligand and metal complexes. The ligand L shows C=O and C=N stretching frequencies around 1627 cm^{-1} and 1597 cm^{-1} (Fig.S3). These stretching frequencies are shifted towards the lower wavelength from 1620-1606 cm^{-1} to 1590-1575 cm^{-1} in all the metal complexes. This shows that, these functional groups from ligand L are involved in complex formation with transition metal ion. This abate in the frequency is due to lowering of electron density *i.e.*, red shift around co-ordination centre C=O and C=N in ligand L (Abdel Rahman *et al* ., 2017 ; Nakamoto, 1977). A few new bands are observed at all metal complexes around 515-520 cm^{-1}, 425-438 cm^{-1} and 357-362 cm^{-1} which are due to the formation of M-O, M-N and M-Cl bonds (Fig. S4). These bands are absent in IR spectrum of ligand L. The ligand shows a broad peak in the region of 3420 cm^{-1} which is due to enolic OH group which is completely disappeared due to complex formation. In the FT IR spectra of metal complexes only a sharp band is observed at 3500 cm^{-1} which is due to phenolic OH group in curcumin.

3.4 NMR spectroscopic evidence

In NMR spectroscopy, some peaks are shifted either upfield or downfield after complex formation. The NMR spectra of the ligand and its [ZnLCl] were recorded at room temperature in DMSO-d_6 solvent. ^{1}H NMR spectrum of the ligand (Fig. S5) shows singlet at 2.5 ppm, 3.2 ppm, 3.92 ppm, 5.95 ppm, 10.88 ppm, which are due to CH proton, NH proton, OCH_3 proton, active –CH proton (between C=N and OH) and enolic OH group respectively. It also shows a doublet of doublet at 6.5 and 6.8 which is due to -C=CH group and multiplet at 7.5-8 ppm which is due to aromatic groups present in the ligand L. In ^{1}H NMR spectrum of the [ZnLCl] complex (Fig. S6), the enolic OH singlet peak is absent. This corroborates the coordination of enolic OH of curcumin derived hydrazone with Zn metal ion (Raman & Porkodi 2018).

^{13}C NMR spectrum of ligand (Fig. S7) displays C=C signal at 55.0 ppm, C-H active peak at 78.0 ppm, -C=CH at 110 ppm, C-OH enolic group at 100 ppm, C=O carbon signal at 182.3 ppm, C=N carbon signal at 163.8 ppm and aromatic carbon signals around 120-139.8 ppm. In Zinc complex (Fig. S8) these signals are shifted towards upfield, C=O signal is shifted to 179.2 ppm and C=N signal is shifted to 159.5 ppm. These too corroborate the coordination of C=O and C=N of the ligand L to the Zinc metal ion.

3.5 ESI (Electron Spray Ioniser) Mass analysis

In positive ion mode the ESI mass spectra of both ligand L and copper complex are enumerated which are in good accord with the contingent stoichiometry. The mass spectrum of the copper complex is exposed in Fig.S9. The ligand L advertises a molecular ion peak at m/z 487.5 which corresponds to the molecular formula of the curcumin derived hydrazone $[C_{27}H_{25}N_3O_6]^+$. The copper complex displays a molecular ion peak at 585 m/z and 587 m/z (isotopic peak of chlorine) which coincide with the molecular formula $[C_{27}H_{24}N_3O_6CuCl]^+$. This spectrum also exhibits a few fragment ion peaks at 507.29 m/z, 438.46 m/z, 413.26 m/z, 301.13 m/z and 235.08 m/z which are attributed due to the formation of $[C_{22}H_{20}N_2O_6CuCl]^+$, $[C_{20}H_{19}O_5CuCl]^+$, $[C_{20}H_{19}O_5Cu]^+$, $[C_{20}H_{16}O_3]^+$ and $[C_{19}H_{11}]^+$ ions respectively. From the molecular ion peak and fragment ion peaks the contemplated formula is well congruity with contemplated structure. Further, this provokes the other spectral data and the structure of the complex is confirmed.

3.6 EPR spectra

The X- Band spectrum of copper complex recorded at 300 K in solution state (DMSO) is shown in Fig.S10. In this, the copper complex displays four resolved peaks in low filed region and one resolved peak in high field region. The magnetic moment value of the copper complex shows that it is monomeric in nature. The spin Hamiltonian parameters of the copper complex are calculated and encapsulated in Table 1. The copper complex exhibits characteristic axially g- tensor values $g_{\|}$ 2.282) > $g_{\perp}$ (2.063) > ge (2.0023) and $A_{\|}$ 132) > $A_{\perp}$ indicating copper ion is having square planar coordination (Raman, *et al*., 2018). $g_{\|}/A_{\|}$ is 172 cm^{-1} which is clearly evident that the copper complex is having a non-distorted square planar geometry.

TABLE 1 The spin Hamiltonian parameters of the [CuLCL] complexes in DMSO solution at LNT.

Complex	**g-tensor**			**A × 10^{-4} (cm^{-1})**			**$g_{\|}$/ $A_{\|}$**	**G**
	$g_{\|}$	**$g_{\perp}$**	**g_{iso}**	**$A_{\|}$**	**$A_{\perp}$**	**A_{iso}**		
[CuLCl]	2.282	2.063	2.14	167	45	62	172	4.47

G indicates the measurement of the exchange interaction between multiple copper centers. From the prior reports, it has been revealed that, G is greater than four (G > 4) denotes that the local tetragonal axis exists in the parallel alignment or slightly misaligned. If the value of G is less than four (G < 4), there is a significant exchange coupling existing in between the two metal centers. The G value for the present complex is 4.47 which denotes that the Cu(II) complex exists in parallel alignment or slightly distorted and the monomeric nature of it is confirmed (Arunadevi *et al*., 2017).

3.7 *In Vitro* examination

3.7.1 DNA disentangle studies

3.7.1.1 UV- Vis titration

UV- Vis spectroscopy is one of the vital techniques adopted to see the nature of binding between the CT DNA (Calf Thymus) and metal complexes (Abdel-Rahman, *et al* .,

2013; Biswas, et al., 2018), The absorption spectra of 10^{-3} M solution of metal complexes (dissolved in DMSO) are recorded in the presence as well as in the absence of CT DNA. All the metal complexes bind with CT DNA and exhibit $\pi \rightarrow \pi^*$ transition near 255- 260 nm. Due to the damage of the double helical structure of CT DNA by the metal complex, hyperchromic bands are appeared during the successive addition of 30 µL of CT DNA with the metal complexes. These hyperchromic bands of the cobalt complex are displayed in Fig.1. This confirms the groove mode of binding between the CT DNA and metal complexes (Gaber *et al.*, 2018).

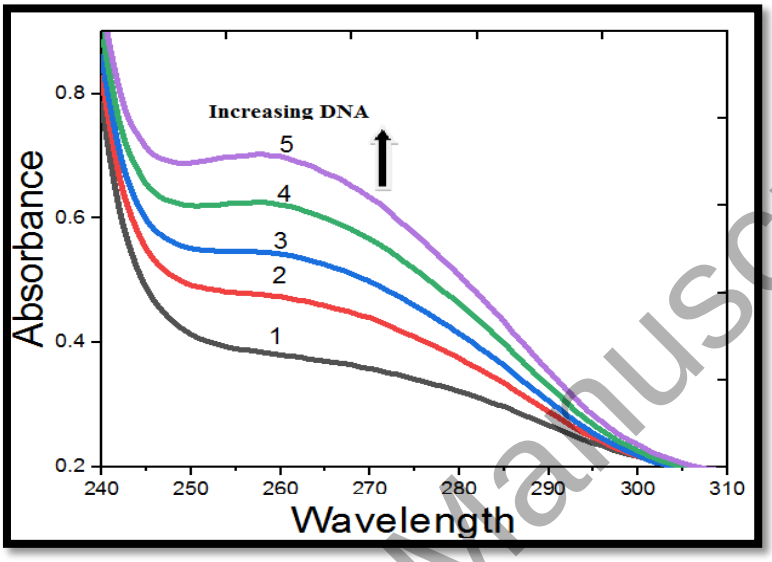

Fig. 1. The absorption spectra of the [CuLCl] complex in buffer (pH =7.2) at 25 °C in presence of increasing amount of DNA. Arrow indicates the changes in absorbance upon increasing the DNA concentration

Intrinsic binding constant (K_b) was calculated for all the metal complexes and it was tabulated in Table 2. The order of binding efficiency of the metal complexes is [CuLCl]> [ZnLCl] > [CoLCl] > [NiLCl]. Amid all, higher binding efficiency is shown by copper complex with 2.9 x 10^{-4} M K_b value.

TABLE 2 Electronic absorption parameters for the interaction of DNA with synthesized metal complexes in 10^{-3}mM solution.

Compound	**λ max(nm)**		**Δλ**	**[a]H%**	**$K_b \times 10^4$ (M^{-1})**
	Free	**Bound**	**(nm)**		
L	235	237	2	0.85	1.2
[CuLCl]	255	263	8	3.13	2.9
[NiLCl]	250	255	5	2.0	1.8
[CoLCl]	256	260	4	1.5	1.6
[ZnLCl]	252	258	6	2.3	2.1

[a]H% = $[(A_{free} - A_{bound}) / A_{free}] \times 100\%$

3.7.1.2 Viscosity measurements

Another evidence for the mode of binding interaction between the metal complexes and CT DNA is the viscosity measurement studies. Viscosity of the metal complexes is evaluated at constant CT DNA concentration and concentration of the metal complexes was varied. The relative viscosity of the DNA decreased steadily with incremental addition of metal complexes. Due to the steric and bulky nature of the metal complex, these can bind only in the surface of the CT DNA and makes the drop off in viscosity (Suh & Chaires, 1995) . This also makes an evidence for the groove mode of interaction between the CT DNA and the metal complexes. Heedless of all the complexes, copper complex has higher efficiency to bind with the CT DNA. The viscosity of metal complexes and EB (Ethidium bromide) with CT DNA at 30^{o}C was plotted in Fig. 2.

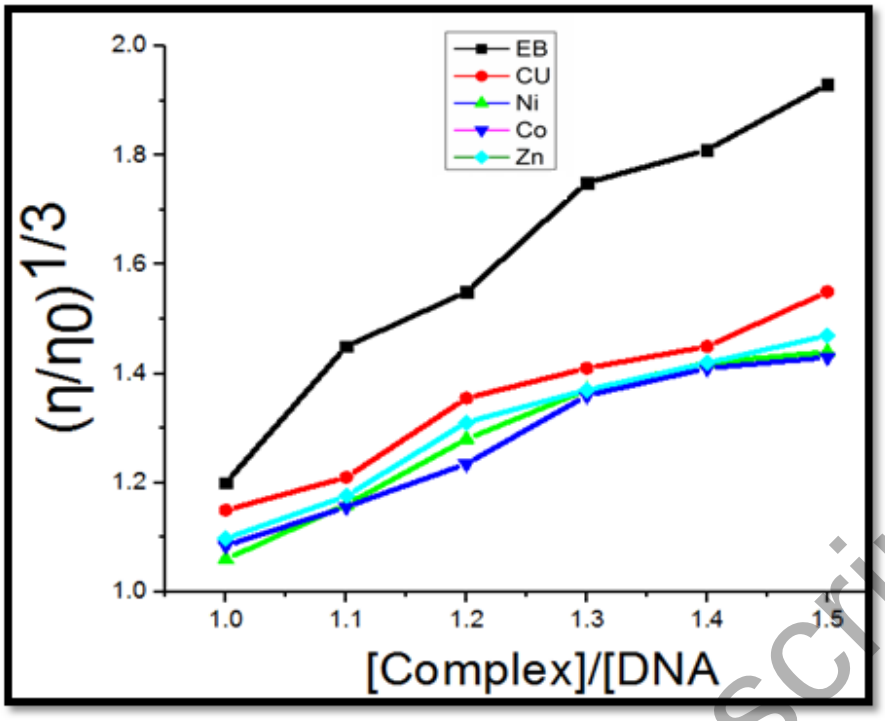

Fig. 2. Effect of increasing amount of [EB] (■), Complexes [CuLCl] (●), [ZnLCl] (◆), [NiLCl](▲) and [CoLCl] (▼) on the relative viscosity of CT DNA. Plot of relative viscosity $(\eta/\eta o)^{1/3}$ *vs* [Complex]/[DNA].

3.7.1.3 CV (Cyclic voltammetry) studies

CV behaviour of the metal complexes in DMSO solution is encountered in presence and absence of the CT DNA with all the synthesized metal complexes. As the concentration of CT DNA increases, there is a change in the potential as well as the anodic and cathodic peaks. During one electron transfer in the redox process of the metal complexes, the value of I_{pc}/I_{pa} (less than unity) provides an evidence for the reaction on the glassy carbon electrode surface which is quasi-reversible. The Table 3 offers the calculated shifts of the cathodic (E_{pc}) and anodic (E_{pa}) potentials and quasi-reversible redox couples upon the addition of CT DNA in Tris–HCl and NaCl buffer solution to the [CuLCl].

TABLE 3 CV calculated data for the interaction of CT- DNA with synthesized metal complexes in 10^{-3} mM solution.

Complex	$E_{1/2}$(V)[a]		[b]$\Delta Ep(V)$		Ip_a/Ip_c
	Free	Bound	Free	Bound	
[CuLCl]	0.436	-0.511	0.695	1.189	-0.76
[NiLCl]	0.125	0.105	0.476	0.653	0.34
[CoLCl]	0.238	0.167	-0.245	0.198	0.46
[ZnLCl]	0.139	0.019	0.108	0.209	0.18

Groove mode of binding between the metal complexes and CT DNA is confirmed by the decrease in anodic and cathodic peak current in CV analysis as well as the E_{pc} and E_{pa} values are moved towards the negative side (Sirajuddiin *et al*., 2013). The CV behavior of the copper complex in presence and absence of CT DNA is displayed in Fig.3.

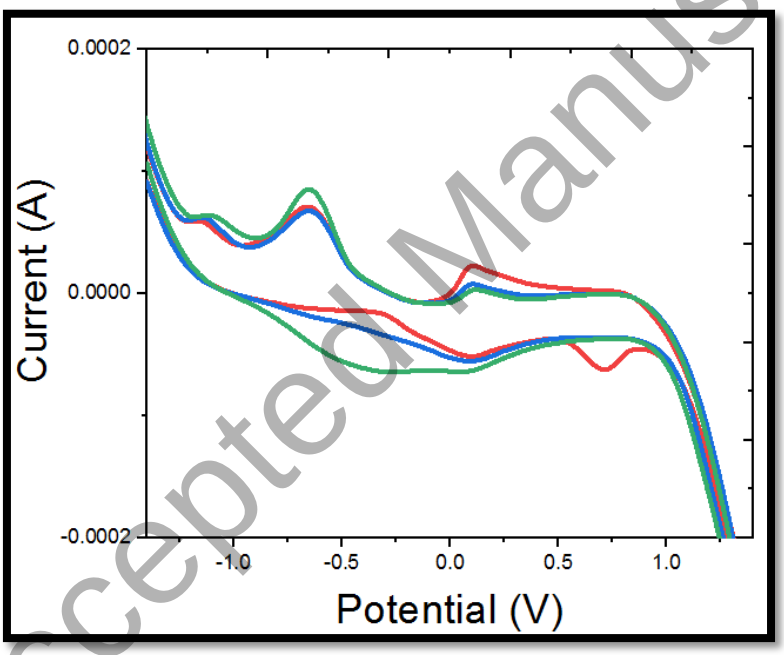

Fig. 3. The cyclic voltammograms of the [CuLCl] complexes in buffer (pH = 7.2) at 25^0C in presence of increasing amount of DNA.

3.7.1.4 DNA cleavage studies

DNA cleavage efficiency of the ligand L and its transition metal complexes against pUC 19 (Plasmid University of California) DNA has been evaluated by agarose gel electrophoresis technique in presence of H_2O_2 as an oxidant. During this method, the fastest cleavage will be the form I (supercoiled stage). Then after this cleavage, a slow relax

cleavage form II (nicked form) is generated. Form III (linear stage) is generated at the last (Sundaravadivel *et al*., 2018). Fig.4 clearly explores that all the metal complexes have the ability to cleave the pUC 19 DNA. This is due the presence of H_2O_2 (oxidizing agent). This reacts with the metal complexes and liberates hydroxyl or super oxide radical. These reactive oxygen species aided in the oxidation of nucleosides units and incision the pUC19 DNA (Uma *et al*., 2005; Dhar *et al*., 2006).

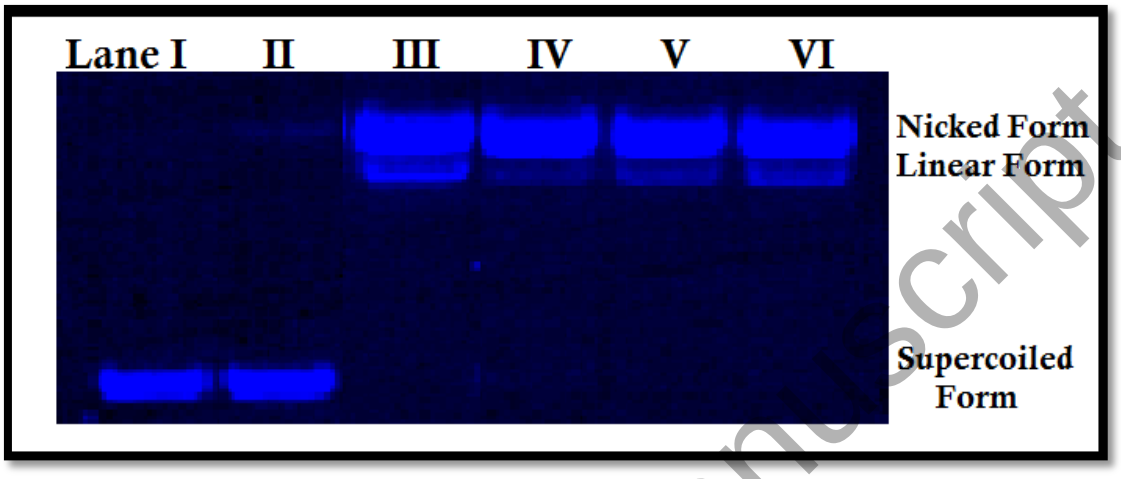

Fig.4. Gel electrophoresis pattern showing cleavage of pUC19 DNA treated with metal complexes: Lane I: DNA control; Lane II: DNA + L+ H_2O_2; Lane III: DNA + [CuLCl] + H_2O_2; Lane IV: DNA + [NiLCl] + H_2O_2; Lane V: DNA + [CoLCl] + H_2O_2 and Lane VI: DNA + [ZnLCl] + H_2O_2.

3.7.1.5 Antimicrobial screening

Transition metal complexes from biological origin acquire higher activity toward the microbial organisms without any side effects. Using broth dilution method, antimicrobial activity is screened in Gram-negative and Gram-positive bacteria and five different strains of fungi and it is tabulated in Tables 4 and 5. From the tables, it is discerned that all the metal complexes demonstrate great antimicrobial activity than the ligand L and they have nearly similar reactivity with the standard. The order of activity is [CuLCl]>[ZnLCl]> [NiLCl] > [CoLCl].

TABLE 4 Minimum inhibitory concentration of the synthesized ligand and metal complexes against the growth of bacteria (μM).

Compound	**MIC values (× 10^{-3} μM) SEM= ±1.2**				
	Staphylococcus aureus	*Bacillus subtilis*	*Salmonella typhi*	*Klebsiella pneumoniae*	*Escherichia coli*
L	10.3	11.6	11.7	13.0	12.6
[CuLCl]	3.1	3.5	3.1	3.8	3.2
[NiLCl]	4.5	4.2	4.4	5.2	5.6
[CoLCl]	4.0	3.9	4.2	4.9	4.7
[ZnLCl]	4.9	4.0	5.1	4.4	4.9
Streptomycin	1.2	1.5	2.0	2.3	2.0

TABLE 5 Minimum inhibitory concentration of the synthesized ligand and metal complexes against the growth of fungi (μM).

Compound	**MIC values (× 10^{-3} μM) SEM= ±1.0**				
	Aspergillus niger	*A.flavus*	*Curvularia lunata*	*Rhizoctonia bataticola*	*Candida albicans*
L	20.4	22.1	20.6	21.5	22.7
[CuLCl]	11.2	11.1	11.4	12.1	11.5
[NiLCl]	13.5	14.2	15.4	14.7	14.5
[CoLCl]	14.5	13.7	14.3	14.6	14.1
[ZnLCl]	12.3	12.4	12.7	13.1	12.3
Fluconazole	3.1	3.4	4.5	3.9	4.0

3.8 *In Silico* calculations

3.8.1 Examination of ADMET properties

SWISS ADME predictor online software is used to calculate the drug like properties of all the synthesized compounds. The pharmacokinetics behavior of the synthesized compounds is displayed in table 6.

TABLE 6 *In silico* ADMET examination of the ligand and its metal complexes

Compounds	Physico Chemical properties					Bioactivity score
	mi log p	TPSA A^0	No. of H bond acceptors	No of H bond donars	No of rotatable bonds	
L	2.60	93.04	6	2	10	0.55
[CuLCl]	1.51	122.50	7	3	7	0.55
[NiLCl]	1.78	122.50	7	3	7	0.55
[CoLCl]	1.78	122.50	7	3	7	0.55
[ZnLCl]	1.78	122.50	7	3	7	0.55

According to Lipinski'rule, the molecule with Log P value below 5 should have drug like character. All the synthesized compounds have Log P less than 5 which implies that, they have higher tendency to penetrate into the biological membrane. TPSA (Total Polar Surface Area) parameter helps us to predict the way of drug transport inside the various parts of the body like gastrointestinal tract, blood brain barrier (BBB), cell membrane and oral bioavailability. It is analyzed by hydrogen bonding ability of the molecules. The TPSA values of curcumin Schiff base and metal complexes are 93.04 A^0 and 122.5 A^0 which are below 140 A^0 (Veber's rule) (Veber *et al.*, 2002). This implies the efficient transport of the synthesized compounds inside the intestine and BBB (Lipinski *et al*., 1997).

The number of hydrogen donors and the number of hydrogen bond acceptors for the synthesized compounds are less than 5 and less than 10 respectively, which reveal that they are active in oral mode of administration also. Moreover, the synthesized compounds also have fewer numbers of rotatable bonds (≤10 according to Veber's rule) which also support the oral bioavailability of the synthesized compounds. The biological active of the synthesized compounds are also supported by their bioactivity score 0.55 (greater than 0 according to Lipinski ' rule) and non-toxicity character.

3.8.2 Quantum chemical studies

DFT analysis of the synthesized compounds has been studied using Gaussian 09 W program. Optimized geometries and stabilization energy of these compounds are analyzed using B3LYP (Becke *et al.*, 1988; Selmi *et al*., 2018; Nielsen *et al*., 2004; Machura *et al*., 2008). The electron density of ligand and the metal complexes are mainly distributed over the C=N, C=O and enolic OH group moiety. The stability and electronic structure of the synthesized complexes had been evaluated by analyzing the highest occupied molecular orbital (HOMO) and lowest unoccupied molecular orbitals (LUMO). The HOMO and LUMO of CuLCl and ZnLCl are displayed in Fig. 5**.** In all the complexes, HOMO electron density distribution is extended to the metal ion and chloride ion. The LUMO electron density of all complexes is well distributed over the co-ordination site except the chloride ion. In general, the aromatic rings in curcumin are not significantly involved in the HOMO electron density distribution. This reveals that these metal complexes have the efficiency to interact with electrophilic species through the region around metal-ligand bonds (Ekennia *et al*., 2017).

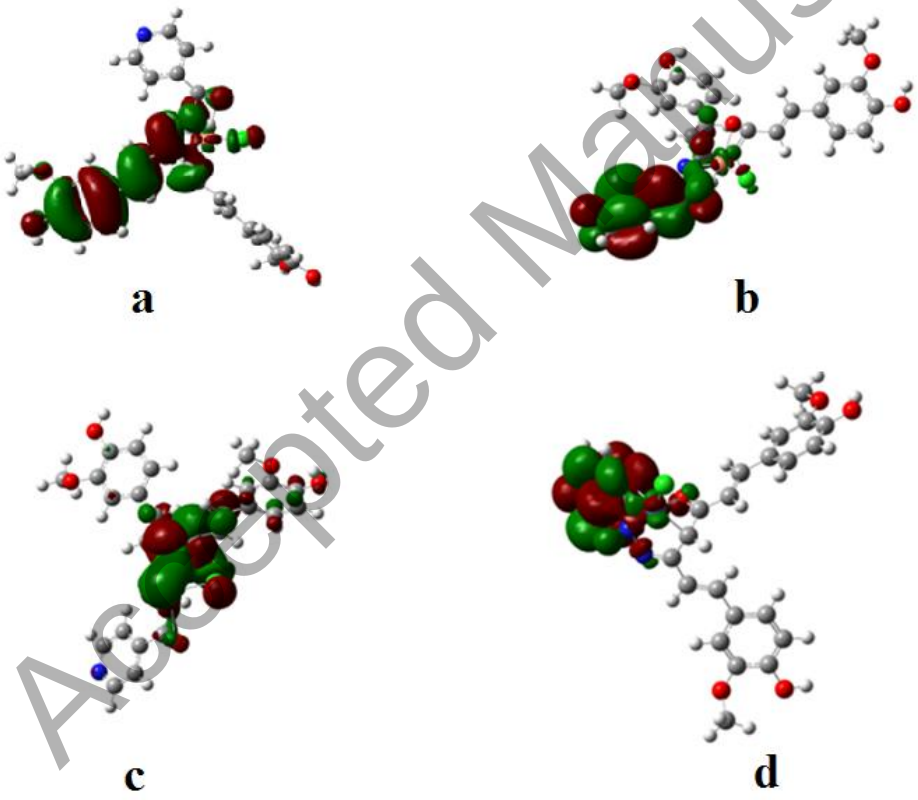

Fig.5. HOMO LUMO of copper and zinc complexes

(a) HOMO of copper complexes (b) LUMO of copper complexes

(c) HOMO of zinc complexes (d) LUMO of zinc complexes

From the HOMO and LUMO values, energy gap, electronegativity, Global hardness, Global softness and electrophilicity index are calculated and tabulated in Table **7.**

TABLE 7 Molecular mechanics data of ligand and its metal complexes in Gaussian Software 09W

Parameter	Ligand	[CuLCl]	[CoLCl]	[NiLCl]	[ZnLCl]
ΔH_f	-1650.14	-3758.26	-3483.34	-3608.80	-3897.46
Dipole moment (Debye)	6.4867	15.7135	10.235	9.4867	12.27
HOMO	-0.19907	-0.21862	-0.18608	-0.18520	-0.19304
LUMO	-0.06528	-0.15857	-0.09443	-0.11053	-0.11825
ΔE (eV)	0.9317	**0.**06005	0.09165	0.07467	0.098946
Electronegativity (χ) eV	0.132175	0.18859	0.140255	0.147865	0.155645
Global hardness (η)	0.066895	0.09429	0.045825	0.03733	0.04947
Global softness (S)	14.9488	10.6047	21.8221	26.7881	20.2142
Electrophilicity (ω)	0.13057	0.18859	0.21463	0.29284	0.24484

Heat of formation value is higher for zinc complex which implies that it is formed more spontaneously than the other complexes. The order of stability is [ZnLCl] > [CuLCl] > [NiLCl]> [CoLCl]. Energy gap ΔE represents the kinetic stability and reactivity pattern of the molecule. According to Pearson, this energy gap represents the chemical hardness of the molecule. According to Maximum Hardness Principle, "there seems to be a rule of nature that molecules arrange themselves so as to be as hard as possible, namely chemical hardness can be considered as measure of the stability". Copper complex has low energy gap ΔE and higher hardness than the other compounds. This reveals that it has low kinetic stability and high chemical reactivity than the other compounds (Pearson, 1987).

Using the DFT calculation, dipole moment is also evaluated for the synthesized compounds. Higher the dipole moment in a molecule, higher will be the biological interactions. Copper complex has higher dipole moment and so it will have a better interaction with the biological system which is proved by antimicrobial examination studies (Ekennia *et al*., 2017).

3.8.3 PASS – Biological activity prediction of curcumin derived hydrazone

The biological activity of the curcumin derived hydrazone L is predicted by means of PASS online software. From the P_a value (probability of active value), it is found that the ligand L acts as a growth stimulant (P_a value 0,917) and it also acquires anti- mycobacterical activity (P_a value 0,848) than the free curcumin. The biological activity given by the software is exposed in Table 8.

TABLE 8 Bioactivity of curcumin derived hydrazone predicted using PASS online software

P_a	**Pi**	**Activity**
0,917	0,001	Growth stimulant
0,848	0,003	Antimycobacterial
0,713	0,008	Preneoplastic conditions treatment
0,699	0,004	Antituberculosic
0,503	0,009	Prostate cancer treatment
0,509	0,069	Antineoplastic
0,444	0,007	Anti-Helicobacter pylori
0,454	0,021	Antibacterial
0,402	0,046	Antiviral (Influenza)
0,420	0,064	Apoptosis agonist
0,321	0,020	Antioxidant

Pa- probability of active Pi- probability of inactive

3.8.4 Molecular Docking studies

Optimised binding mode between the receptor and metal complex has been screened by Molecular Docking studies. Based on the P_a value retrieved from the PASS biological activity prediction software, the receptor *trans* enoyl acyl carrier reductase inhibitor which is responsible for the anti mycobacterical activity is found out. Its 3D structure is downloaded from protein data bank. Its water and NADH molecules are removed from discovery studio 4.0 software. Molecular docking studies are carried out between the *trans* enoyl acyl carrier reductase enzyme and the synthesized compounds. The Docking Score for the all the metal complexes is higher when compared to that of the ligand L. The Docking Score for the ligand L, copper(II), cobalt(II), nickel(II) and zinc(II) complexes is as follows: -363.6 kJ mol^{-1}, -393.15kJ mol^{-1}, - 377.4 k J mol^{-1}, - 381.1 kJ mol^{-1} and - 379.1 kJ mol^{-1} respectively. All the metal complexes have higher affinity to bind with the *enoyl acyl carrier reductase* inhibitor by H-bonding with amino acids than the ligand. Docking images of copper and cobalt complexes are displayed in Fig. 6a and Fig.6b**.**

To confirm the groove mode of binding between the DNA and metal complex, 1BNA crystal structure was retrieved from PDB. The ligand and all the metal complexes were docked with 1BNA and the docking pictures are shown in Fig 6c and Fig.6d**.** All the metal complexes exhibit higher binding score than the ligand value. The Docking score for the ligand L, copper(II) , cobalt(II), nickel(II) and zinc(II) complex with 1BNA is as follows: -333.6 kJ mol^{-1}, -363.15kJ mol^{-1}, - 367.4 k J mol^{-1}, - 351.0 kJ mol^{-1} and - 359.1 kJ mol^{-1} respectively. These docking studies are also evident for the groove mode of binding between the DNA and metal complexes.

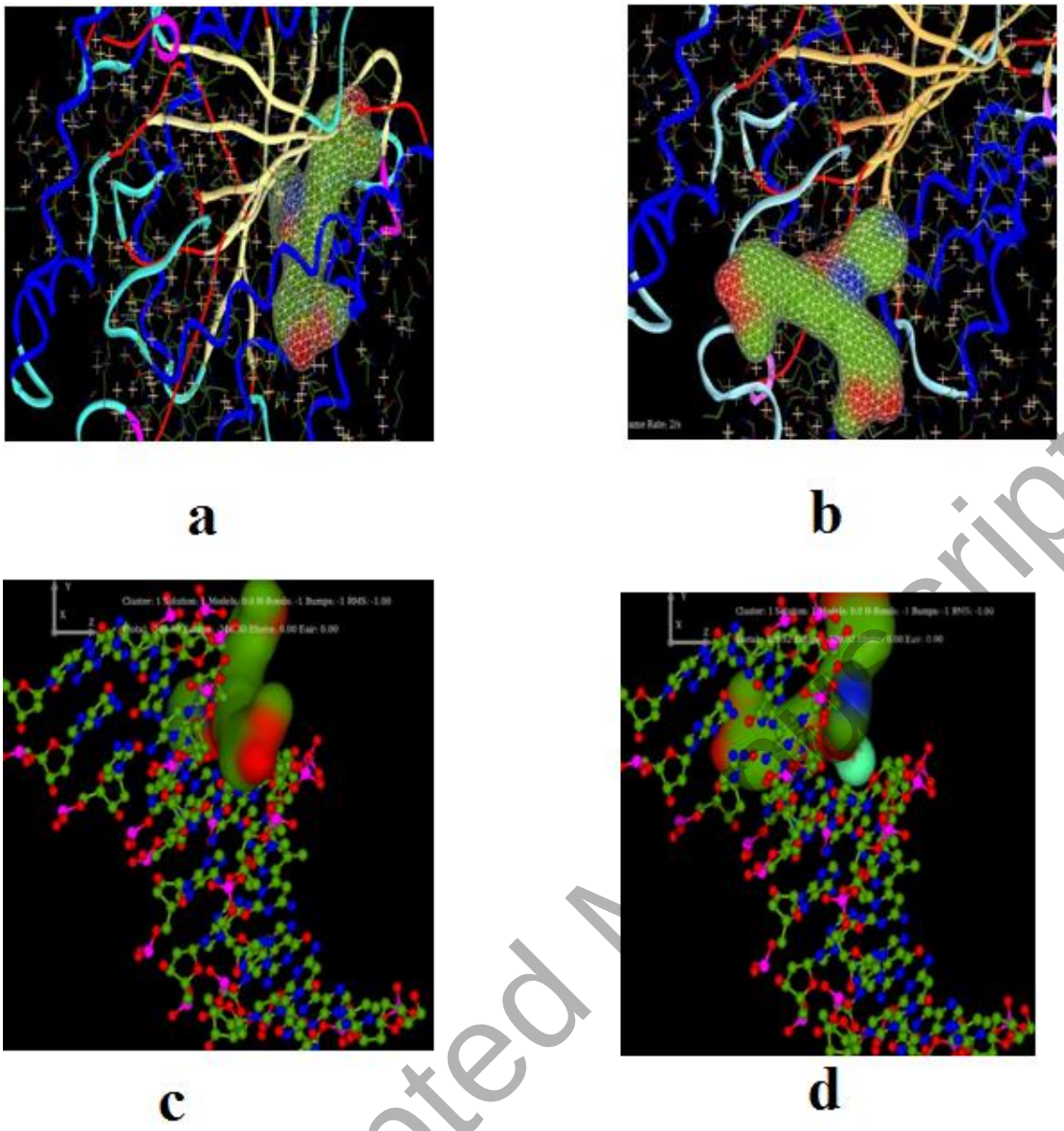

Fig. 6. Docking model of copper (a) and nickel (b) complexes with *trans enoyl acyl carrier reductase* inhibitor and copper (c) and cobalt (d) complexes with 1BNA

4 Conclusion

In the present study, new transition metal complexes from curcumin derived hydrazone are synthesized and characterized. The coordination sites between the ligand and metal complexes are confirmed by IR and NMR spectral studies. The geometry of the metal complexes is corroborated by evaluating electronic, magnetic moments, EPR and ESI Mass analyses. Groove mode of binding between the CT DNA and the metal complexes is corroborated by electronic spectroscopy, CV and viscosity measurements. All the complexes

have potent to cleave pUC 19 DNA and so they can be developed into anticancer agents. *In silico* ADMET properties of the synthesized compounds reveal higher biological potential and oral administrative activity. DFT calculation advocates the optimized geometry, chemical hardness, dipole moment of the synthesized compounds. This reveals that copper(II) complex explores higher stability and higher biological accessibility. PASS online biological activity prediction software of ligand exhibits higher anti-mycobacterical activity than curcumin. Molecular docking studies also supports the groove mode of binding between the 1BNA and synthesized compounds and copper complex has higher binding efficiency towards the target than other compounds. *In vitro* studies of the metal complexes show propitious antimicrobial activities comparing to ligand L.

Acknowledgments

The authors express their sincere thanks to the Management, Principal and Head of the Department of Chemistry, VHNSN College and The Standard Rajaratnam College for Women, Sivakasi for providing necessary facilities to do this research work. IIT Bombay is admiringly recognized for providing instrumental facilities. We also extended our sincere thanks to Department of Science and Technology, New Delhi for the financial assistance (Gaussian Software 09W).

References

Abdel-Rahman, L. H.; El-Khatib, R. M.; Nassr, L. A. E.; Abu- Dief, A. M.; Lashin, F. E., (2013). Design, characterization, teratogenicity testing, antibacterial, antifungal and DNA interaction of few high spin Fe (II) Schiff base amino acid complexes, *Spectrochim. Acta Part A.* 111, 266 – 276.

Biswas, N et al (2018), Example of two novel thiocyanato bridged copper (II) complexes derived from substituted thiosemicarbazone ligand: structural elucidation, DNA/albumin binding, biological profile analysis, and molecular docking study, *J. Biomol Struct Dyn*. https://doi.org/10.1080/07391102.2018.1503564.

Abdel-Rahman, L.H., Abu-Dief, A.M., El-Khatib, R.M., Abdel- Fatah, S.M., (2016). Sonochemical synthesis, DNA binding, antimicrobial evaluation and in vitro anticancer activity of three new nano-sized Cu(II), Co(II) and Ni(II) chelates based on tridentate NOO imine ligands as precursors for metal oxides. *J. Photochem. Photobio.* B 162 298–308.

Abu-Dief, A. M. and Nassr, L. A. E., (2015). Tailoring, physicochemical characterization antibacterial and DNA binding mode studies of Cu(II) Schiff bases amino acid bioactive agents incorporating 5-bromo-2-hydroxybenzaldehyde , *J. Iran. Chem. Soc.*, 12, 943-955.

Abdel Rahman, L.H., Abu-Dief, A.M., Moustafa, H., Hamdan, S.K., (2017). Ni(II) and Cu(II) complexes with ONNO asymmetric tetradentate Schiff base ligand: synthesis, spectroscopic characterization, theoretical calculations, DNA interaction and antimicrobial studies. *Appl. Organometal. Chem.* 31 e3555.

Annaraj, J., Srinivasan, S., Ponvel, K.M., Athappan, P. R., (2005). Mixed ligand copper(II) complexes of phenanthroline/bipyridyl and curcumin diketimines as DNA intercalators and their electrochemical behavior under Nafion and clay modified electrodes, J. *Inorg. Biochem.* 99(3), 669–676.

Anjaneyulu, Y., Rao, R. P., (1986). Preparation, Characterization and Antimicrobial Activity Studies on Some Ternary Complexes of Cu(II) with Acetylacetone and Various Salicylic Acids, *Synth. React. Inorg. Org. Chem.*16(2), 257-272.

Arunadevi, A., Paulpandiyan, R., Raman, N., (2017). DNA interaction, molecular docking and biological profile of tetradentate histidine based metallointercalators, *J.Mol.Liq.* 241(0), 801-810.

Awasthi, M., Swati, Si., Veda, P. P., and Upendra, N. D., (2018). Modulation in theconformational and stability attributes of the Alzheimer's disease associated amyloid-beta mutants and their favorable stabilization by curcumin: molecular dynamics simulation analysis, *J Biomol Struct Dyn.* , 36(2) 407-422, DOI: 10.1080/07391102.2017.1279078.

Barbier, J. P., Biyyadh, A. E., Kappenstein, C., Dongui Mabiala, N., Hugel, R. P., (1985). Square-planar complexes of copper(II), nickel(II), and cobalt(II) with deprotonated biuret derivatives. Crystalline and molecular structures of sodium (o-phenylene and propylenebis(biuretato)cuprate(II)-dimethyl sulfoxide complexes, *Inorg. Chem.* 24 (22), 3615–3620.

Becke, A. D., (1988). Density-functional exchange-energy approximation with correct asymptotic behavior, *Phys. Rev. A.* 38, 3098–3100.

Blasco, S., Burguete, M. I., Clares, M. P., Garcia-Espana, E., Escorihuela, J., Luis, S. V., (2010). Coordination of Cu^{2+} Ions to C_2 Symmetric Pseudopeptides Derived from Valine, *Inorg. Chem.* 49(17), 7841-7852.

Chanphai, P., and Tajmir-Riahi, H.A. (2018). Binding analysis of antioxidant polyphenols with PAMAM nanoparticles, *J Biomol Struct Dyn.* 36(13) 3487-3495, DOI: 10.1080/07391102.2017.1391124

Cheng, A.L. , Hsu, C.H., Lin, J.K., Hsu, M.M., Ho, Y.F., Shen, T.S., Ko, J.Y., Lin, J.T., et al., (2001). Phase I clinical trial of curcumin, a chemopreventive agent, in patients with high-risk or pre-malignant lesions, *Anticancer Res.* (21), 2895-2900.

Dhar, S., Nethaji, M., Chakravarty, A. R., (2006). DNA Cleavage on Photoexposure at the d−d Band in Ternary Copper(II) Complexes Using Red-Light Laser, *Inorg. Chem.* 45 (26), 11043-11050.

Ekennia, C.A., Osowole, A.A., Olasunkanmi, L.O., Onwudiwe, D.C., Olubiyi, O.O., Ebenso, E.E.,(2017). Synthesis, characterization, DFT calculations and molecular docking studies of metal (II) complexes, *J.Mol.Struct.* 1150, 279-292.

Fekri, R., Salehi, M., Asadi, A., Kubicki, M., (2018). Spectroscopic studies, structural characterization and electrochemical studies of two cobalt (III) complexes with tridentate hydrazone Schiff base ligands: Evaluation of antibacterial activities, DNA-binding, BSA interaction and molecular docking, *Appl.Organomet.Chem.* 32 (2), e4019.

Ferraresi-Curotto,V., Echeverria,G.A., Piro, O.E., Pis-Diez, R., Gonzalez-Baro, A.C., (2015). Structural, spectroscopic and DFT study of 4-methoxybenzohydrazide Schiff bases. A new series of polyfunctional ligands, *Spectrochim. Acta Part A.*137, 692-700.

Ferreira, M. L., Goncalves, R. S. B., Cardoso, L. N. F., Kaiser, C. R., Candea, A. L. P., Henriques, M. G. M. O., Lourenco, M. C. S., Bezerra, F.A. F. M., De Souza, M. V. N., (2010). Synthesis and Antitubercular Activity of Heteroaromatic Isonicotinoyl and 7-Chloro-4-Quinolinyl Hydrazone Derivatives, *Sci. World. J.* 10, 1347–1355.

Gaber, M.H., Ghamry, A. E., Fathalla, S. K., Mansour, M.A., (2018). Synthesis, spectroscopic, thermal and molecular modeling studies of Zn^{2+}, Cd^{2+} and UO_2^{2+} complexes of Schiff bases containing triazole moiety. Antimicrobial, anticancer, antioxidant and DNA binding studies, *Mater. Sci. Eng. C.* 83, 78-89.

Geary, W. J., (1971). The use of conductivity measurements in organic solvents for the characterisation of coordination compounds, *Coord. Chem. Rev.*7(1), 81-122.

Goel, A., Kunnumakkara, A. B., Aggarwal, B., (2008). Curcumin as "*Curecumin*": From kitchen to clinic, *Biochem. Pharmacol.* 75(4), 787- 809.

Gonzalez-Baro, A. C., Pis-Diez, R., Parajon-Costa, B.S., Rey, N.A., (2012). Spectroscopic and theoretical study of the *o*-vanillin hydrazone of the mycobactericidal drug isoniazid, *J. Mol. Struct.* 1007, 95–101.

Gonzalez-Baro, A. C., Veronica Ferraresi, C., Diez, R. P., Resende, J. A. L. C., Parajon Costa, B.S., De Paula, F. C. S., Pereira-Maia, E. C., Rey, N.A., (2017). A novel oxidovanadium(V) compound with an isonicotinohydrazide ligand. A combined experimental and theoretical study and cytotoxity against K562 cells, *Polyhedron.*135, 303-310.

Heger, M., Van Golen, R.F., Broekgaarden, M., Michel, M. C., (2014). The Molecular Basis for the Pharmacokinetics and Pharmacodynamics of Curcumin and Its Metabolites in Relation to Cancer, *Pharmacol. Rev.* 66 (1), 222-307.

Heinrich, J., Stubbe, J., Kulak, N., (2018). Cu (II) complexes with hydrazone-functionalized phenanthrolines as self-activating metallonucleases, *Inorganica Chim. Acta.* 481, 79-86.

Jaykant Vora, Shivani Patel, Sonam Sinha, Sonal Sharma, Anshu Srivastava, Mahesh Chhabria & Neeta Shrivastava (2018) Molecular docking, QSAR and ADMET based mining of natural compounds against prime targets of HIV, *J Biomol Struct Dyn.* DOI: 10.1080/07391102.2017.1420489

Khan, T., Dixit, S., Ahmad, R., Raza, S., Azad, I., Joshi, S., Rahman Khan, A., (2017). Molecular docking, PASS analysis, bioactivity score prediction, synthesis, characterization and biological activity evaluation of a functionalized 2-butanone thiosemicarbazone ligand and its complexes, *J. Chem. Biol.* 10 **(**3), 91–104.

Krishnamoorthy, P., Sathyadevi, P., Cowley, A. H., Butorac, R. R., Dharmaraj, N., (2011). Evaluation of DNA binding, DNA cleavage, protein binding and *in vitro* cytotoxic activities of bivalent transition metal hydrazone complexes, *Eur. J.Med. Chem.* 46 (8), 3376- 3387.

Lipinski, C. A., Lombardo, F., Dominy, B. W., Feeney, P.J., 1997. Experimental and computational approaches to estimate solubility and permeability in drug discovery and development settings, *J.Adv. Drug Deliv. Rev.* 46 (1-3), 3-25.

Maccar, R., Ottana, R., Bottari, B., Rotondob, E., Vigorita, M. G., (2004). *In vitro* advanced antimycobacterial screening of cobalt(II) and copper(II) complexes of fluorinated isonicotinoylhydrazones, *Bioorganic. Med. Chem. Lett.* 14 (23), 5731–5733.

Nakamoto, K., Wiley Interscience, III Edition, New York, (1977).296 –346.

Nejo, A. A., Kolawole, G. A., Nejo, A. O., (2010). Synthesis, characterization, antibacterial, and thermal studies of unsymmetrical Schiff-base complexes of cobalt(II), *J. Coord. Chem.* 63(24), 4398-4410.

Nielsen, R. J., Keith, J. M., Stoltz, B. M., Goddard, W. A., (2004). A Computational Model Relating Structure and Reactivity in Enantioselective Oxidations of Secondary Alcohols by (-)-Sparteine-PdII Complexes, *J. Am. Chem. Soc.* 126(25), 7967–7974.

Niu, X., Yawen, G., Yiding Yu, Yanan, Y., Guizhen, W., Lin, S., and Hongsu , W., (2018) Molecular Modelling reveals the inhibition mechanism and structure–

activity relationship of curcumin and its analogues to *Staphylococcal aureus* Sortase A, *J Biomol Struct Dyn.* , DOI: 10.1080/07391102.2018.1453380.

Pearson, R. G., (1987). Recent advances in the concept of hard and soft acids and bases, *J. Chem. Educ.* 64(7), 561–567.

Porkodi, J., Raman, N., (2018). Synthesis, characterization and biological screening studies of mixed ligand complexes using flavonoids as precursors, *Appl.Organomet.Chem.* 32(2), e4030.

Pramanik, A. R., Das, D., Paul, P. C., Mondal, P., Bhattacharjee, R., (2014). Newer mixed ligand Schiff base complexes from aquo-N-(2′-hydroxy acetophenone) glycinatocopper(II) as synthon: DFT, antimicrobial activity and molecular docking study, *J. Mol. Struct.* 1059, 309–319.

Raman, N., Chandrasekar, T., Kumaravel, G.,(2018). Synthesis of innovative biochemical active mixed ligand metal(II) complexes with thiazole containing Schiff base: *In vitro* antimicrobial profile, *Appl. Organomet.Chem.* 32 (1), e3922.

Selmi, W., Abdelhak, J., Marchivie, M., Zid, M. F., (2018). A comparative structural, spectroscopic, optical and photoluminescence studies by DFT of Fe(II) difluoro(oxalato)borate complex, *J. Photochem. Photobiol. A*, 352, 43-54.

Shahabadi, N., Kashanian, S., Darabi, F., (2010). DNA binding and DNA cleavage studies of a water soluble cobalt (II) complex containing dinitrogen Schiff base ligand: The effect of metal on the mode of binding, *Eur. J. Med Chem.* 45(9), 4239-4245.

Shebl, M., (2017). Coordination behavior of new bis(tridentate ONO, ONS and ONN) donor hydrazones towards some transition metal ions: Synthesis, spectral, thermal, antimicrobial and antitumor studies, *J. Mol. Struct.*1128: 79-93.

Sigman, D.S., Mazumder, A., Perrin, D.M., (1993). Chemical nucleases, *Coord. Chem. Rev.* 93 (6), 2295.

Sirajuddiin, M., Ali, S., Badshah, A., (2013). Drug–DNA interactions and their study by UV– Visible, fluorescence spectroscopies and cyclic voltametry, *J.PhotochemPhotobiol.B.* 124, 1-19.

Suh, D., Chaires, J. B., (1995). Criteria for the mode of binding of DNA binding agents, *Bioorganic Med. Chem.* 3(6), 723-728

Sundaravadivel, E., Reddy, G.R., Manoj, Rajendarn, S., Kandaswamy, M., Janakiraman, M., (2018) .DNA binding and cleavage studies of copper(II) complex containing N_2O_2 Schiff base ligand, *Inorganica Chim. Acta.* 482, 170-178.

Uma, V., Kanthimathi, M., Weyhermuller, T., UnniNair, B., (2005). Oxidative DNA cleavage mediated by a new copper (II) terpyridine complex: Crystal structure and DNA binding studies, *J. Inorg. Biochem.* 99 (12), 2299-2307.

Varadharajan, T., Kuan-Wei, L., Max K. L., and Ching-Feng, W.,(2018) Potential natural mTOR inhibitors screened by *in silico* approach and suppress hepatic stellate cells activation, *J Biomol Struct Dyn.* 36 (16) 4220-4234, DOI: 10.1080/07391102.2017.1411295.

Veber, D. F., Johnson, S. R., Cheng, H. Y., Smith, B. R., Ward, K. W., Kopple, K. D., 2002. Molecular Properties That Influence the Oral Bioavailability of Drug Candidates, *J. Med. Chem*. 45 (12), 2615–2623.

Xiong, Y., Ji, L.N., (1999). Synthesis, DNA-binding and DNA-mediated luminescence quenching of Ru(II) polypyridine complexes, *Coord. Chem. Rev.* 185,711-733.

Xu, S., Aprahamian, I., (2014). Hydrazone-based switches, metallo-assemblies and sensors**,** *Chem. Soc. Rev.* 43, 1963-1981.